Fabrication and Cooling Performance Optimization of Stretchable Thermoelectric Cooling Device

Ki Mun Bang[†], *Woosung Park*[‡], *Pawel Ziolkowski*[§], *and Hyungyu Jin*[*,†]

[†]Department of Mechanical Engineering, Pohang University of Science and Technology (POSTECH), Pohang 37673, South Korea

[‡]Department of Mechanical Systems Engineering, Sookmyung Women’s University, Seoul 04310, South Korea

[§]German Aerospace Center (DLR) – Institute of Materials Research, Linder Hoehe, 51147 Cologne, Germany

KEYWORDS: stretchable, thermoelectric cooler, heat management, thermal conductivity, elastomer composite

ABSTRACT

Stretchable electronic devices are known as elastic electronics or circuits. They are typically built by deposition or embedding of devices and circuits onto stretchable substrates, which can sustain large strains without failure. The research on this emerging technology has focused on the development of components based on insulators, conductors, or semiconductors in order to overcome inherent difficulties to generate mechanically stable layers and interconnections. Besides the mechanical challenges, the heat dissipation problem remains yet to be solved, since stretchable electronics are generally fabricated using materials with poor thermal conductivities. In order to simultaneously address stretchability and heat dissipation, novel cooling platforms are required. As one promising pathway, this paper presents the fabrication and performance optimization of a thermoelectric device that is stretchable and effectively dissipates heat. The device is easy to fabricate and has a relatively simple structure, consisting of silicone elastomer (Ecoflex), liquid metal, and thermoelectric legs. It is mechanically stable over 1000 cycles of stretching-and-releasing with 30% strain. A thermal analysis reveals that the Ecoflex substrates impose significant thermal resistances to the entire device, degrading its cooling performance. To address the issue, alumina powder is added into the Ecoflex substrates. For the case of Ecoflex/alumina composite substrates with 60 wt. % of alumina, the maximum temperature drop is enhanced by 80% and 50% at 0% and 30% strains, respectively, under no heat load condition. The devices with alumina addition also show a largely improved cooling per unit electrical power input, suggesting their potential merit in cost and energy saving. The cooling capability of the stretchable thermoelectric devices is further confirmed under both conductive and convective heat load conditions.

INTRODUCTION

Stretchable devices are emerging as a next-generation platform for displays and electronic devices.[1-6] Those devices can maintain their functionality while being bent, twisted and stretched. However, the miniaturization of circuits and components involves an associated increase of the electric power density and yields a heat generation during operation, which could severely degrade the durability and electronic characteristics of these devices. Stretchable devices would require completely different heat management solutions than conventional rigid devices owing to their stretchability, but little attention has been paid to methods to dissipate heat from stretchable devices.[7-9]

Removal of heat from electronic devices can use passive or active processes of heat dissipation depending on the heat load characteristics: the former is sufficient in many steady-state heat load conditions, whereas the latter works better when further cooling power is required or when temperatures have to be controlled precisely especially in the case of transient heat load conditions. The passive process uses a metal plate or fins typically in conjunction with a forced convection by an attached fan, whereas the active process uses power input to remove heat. Solid-state thermoelectric (TE) coolers (or Peltier coolers) offer a reliable active cooling operation by means of the Peltier effect.[10] Peltier coolers have raised great attention during the past decades, as they allow for reliable and noiseless operation[11] without moving parts, working fluids, chemical reactions or emissions.[12,13] Peltier coolers have been widely used for thermal management of lasers,[14] microprocessors,[15] and electronic packages.[16,17] However, due to their inflexibility, neither of the above-mentioned passive and active cooling devices is suitable for cooling stretchable electronics. Therefore, new stretchable heat-dissipation strategies are necessary.

One approach is to use a thermally-conductive stretchable material as a passive heat spreader.[18-20] Common stretchable polymers usually have a low thermal conductivity κ [W m^{-1} K^{-1}], but mixing them with materials with high κ (*e.g.*, graphene,[21,21] aluminum oxide,[23-25] boron nitride,[26,27] liquid metal[28-30]) can create a stretchable polymer with an improved κ. These composites may be used as stretchable heat dissipaters.

As a stretchable counterpart of the conventional Peltier cooler, one may devise a stretchable TE device for active cooling. A conventional Peltier cooler is rigid (Figure 1a) as it typically consists of TE legs made of inorganic semiconductors, metal electrodes, and ceramic substrates. These rigid components make the device inapplicable to curved surfaces[31] or stretchable platforms. To address this issue, a new device design consisting of materials that can tolerate deformations needs to be developed. While many attempts have been made over the past decade to demonstrate a flexible TE device that can bend or twist,[32-53] only a few studies have been reported on stretchable TE devices,[54-61] mostly focused on power generation rather than cooling. As for cooling devices, Hong *et al.*[52] have shown a wearable TE device for personalized thermoregulation, which could be heated or cooled during operation, yet the device can only be bent and thus is inapplicable for stretchable platforms. Also, Lee *et al.*[61] have recently demonstrated a skin-like thermo-haptic device based on stretchable TE module, which could be used for wearable virtual reality applications. The very few previous studies have hitherto focused on the fabrication and application aspects of stretchable TE cooling devices. Although careful thermal analysis and design are crucial for developing a high-performance stretchable TE cooling device, such an investigation has been lacking thus far.

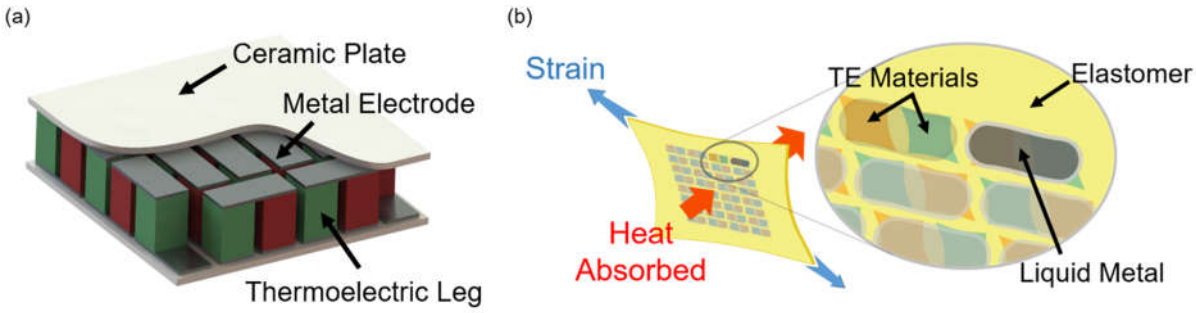

Figure 1. (a) Traditional thermoelectric device. (b) Schematic illustration of stretchable thermoelectric device.

In this work, we propose a stretchable TE cooling device with a relatively simple design (Figure 1b), for which thermal consideration has been taken into account to improve its cooling performance. In our device, stretchable elastomers replace the ceramic substrates, and a liquid metal is used in place of the metal electrodes. We demonstrate that such simple modifications endow the device with considerable stretchability, while maintaining decent cooling performance. We first present the fabrication details of the stretchable TE cooling device, followed by systematic analyses of its electrical and mechanical properties and cooling performance. Through a thermal circuit analysis, we find that the high thermal resistance of the elastomer substrates is a bottleneck to heat flow across the device, degrading its overall cooling capability. We address the issue by introducing a high thermal conductivity filler material into the elastomer, forming a composite with an improved thermal conductivity. We present cooling characteristics and efficiency of those devices with varying filler concentrations under different strains. We also evaluate the cooling performance of several devices under different heat load conditions, in order to verify their applicability to real operation conditions.

EXPERIMENTAL SECTION

Fabrication of Stretchable Thermoelectric Cooling Device

Commercially available Ecoflex was chosen as the substrate material because of its high stretchability.[62] Fabrication (Figure 2) starts with pouring Ecoflex into a mold (Figure 2a). Ecoflex (Ecoflex 00-30, Smooth-On) was prepared by mixing base agent and curing agent in 1:1 weight ratio. The mixture was blended for 5 min using a vortex mixer (neoLab, D-6012), then placed in a vacuum chamber to remove residual bubbles. The prepared Ecoflex was poured into a mold, which was made from a glass slide (Marienfeld), then cured for 5 min at 328 K until the surface had slightly hardened. Then liquid metal (Galinstan, Gallium Indium Tin eutectic 99.99%, Thermo Fisher Scientific Inc.) was transferred on top of the layer as an electrode (Figure 2b). Due to its relatively high thermal conductivity of 16.5 $W \cdot m^{-1} \cdot K^{-1}$ this material has been already used in the past as a liquid coolant within integrated mini- or micro-channel cooling systems.[63-65] Besides its good thermal properties, Galinstan offers a high electrical conductivity of 3.3 $S \cdot \mu m^{-1}$and has a high surface tension of 0.718 $N \cdot m^{-1}$.[63] These properties make it a suitable electrode material for stretchable devices, by providing effective electric conduction and mechanical robustness under stretching. Compared to the eutectic Gallium-Indium (EGaIn) alloy, which is commonly used for stretchable devices, the melting temperature (-19 ^{o}C) of the Galinstan is lower than that of EGaIn (15.5 ^{o}C). Therefore, the use of Galinstan is more suitable for cooling applications. After its application onto the Ecoflex layer TE legs were placed on top of the printed Galinstan. Bi-Te TE legs (cross section area: 1.5 mm x 1.5 mm in area, thickness: 1.0 mm) were prepared by detaching them from a commercial Peltier module (TEC1-12715, Hebei). When the Peltier module was

heated to 523 K using a hotplate, the legs could be easily detached. To prevent oxidization, this process was conducted under Ar. Nine pairs of n- and p- type TE legs were placed one after another onto the Galinstan electrodes to form a series electrical connection. The electric supplying leads were prepared using Cu wires. The tip of each wire was roughened using a sandpaper to increase the wettability with the Galinstan. Two Cu wires were twisted to make one electrical cord, which gave more consistent results compared to the use of a single wire. The Cu wires were placed onto the terminals of the cooling device and additional Galinstan was used to cover the wires in order to create a stable contact. When a large strain is applied, the Cu wires could be detached from the Galinstan contacts, which causes the breakdown of the device. Therefore, thermal cement (OB-600, Omega Engineering) was used to provide additional fixation of the Cu wires (Figure 2c). Next, the Ecoflex was gently poured into the mold until it entirely filled the void spaces next to the TE legs and the configuration was cured for 5 min at 333 K (Figure 2d). After slightly hardening of the surface, additional Galinstan was printed on top of the TE legs to form a series electrical connection throughout the entire device (Figure 2e). Finally, the Ecoflex was poured into the mold until it covered all components of the device and the device was cured for 6 h at 363 K (Figure 2f). The whole fabricated device was removed from the mold to complete the fabrication (Figure 2g and 2h).

The Ecoflex/alumina composite was produced with alumina powder (Sigma-Aldrich, 325 mesh) by mixing it with the Ecoflex base agent. The powder was mixed for 5 min in the vortex mixer, the curing agent was added to the mixture. It was also mixed using the vortex mixer for 5 min, then degassed in the vacuum chamber. The Ecoflex/alumina composite was prepared with different alumina concentrations and used as the top and bottom layers of the tested device (Figure S1).

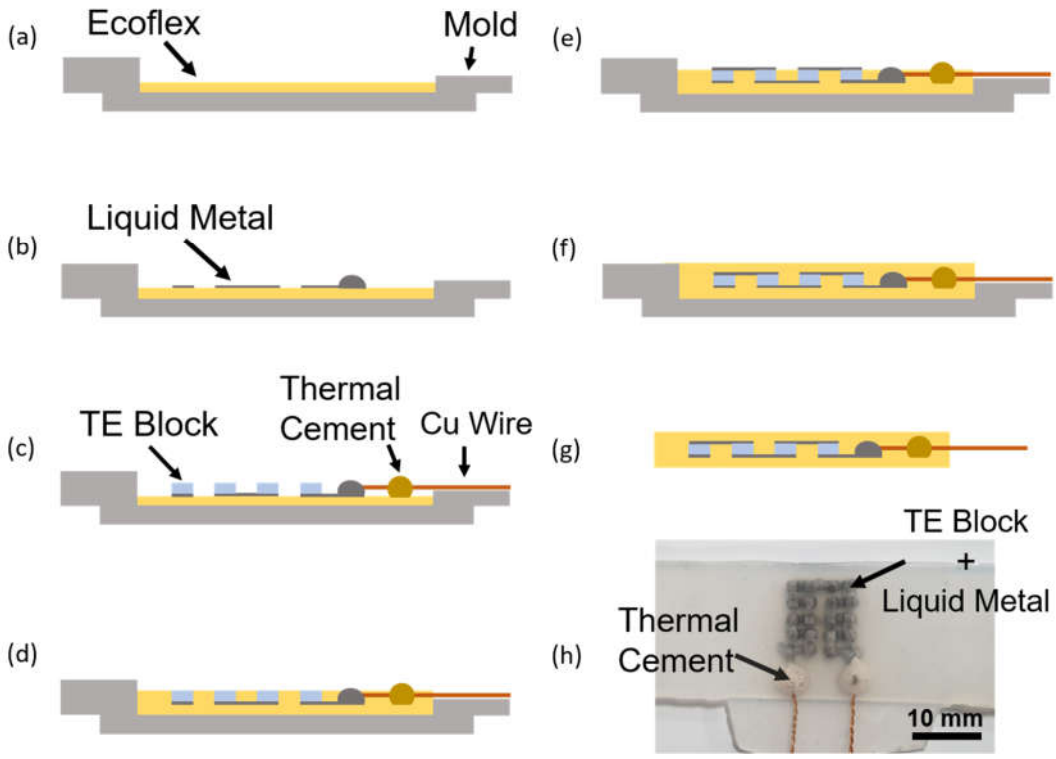

Figure 2. (a-g) Schematic illustration of the process of fabricating the stretchable thermoelectric cooling device. (h) Photograph of the fabricated device.

Characterization

Internal resistance was measured by using four probe method (Lakeshore, Model 372). Strain was applied to each device to check the sensitivity of the internal resistance. To examine the mechanical robustness, resistance was measured during 1000 cycles between 0% and 30% strain.

Strain cycling endurance was measured by using a modular force stage (Linkam, MFS-TST350). Each of the Ecoflex/alumina composite samples was stretched up to 440% strain, and

the 60 wt. % alumina composite sample was repeatedly stretched and released with 30% strain over 1000 cycles to check the mechanical endurance.

Ecoflex/alumina composite samples were formed into 12.7 mm disks with a thickness of 1 mm for the measurement of the thermal diffusivity. The samples were coated with graphite spray and thermal diffusivity was measured by laser flash analysis (Netzsch Instruments Co., LFA 476). Each of the samples was measured 13 times while increasing the temperature by 10 K from 300 K to 380 K, and the distribution of thermal diffusivity was recorded (Figure S2). The density was measured using Archimedes' method (Mettler Toledo, Balance XS105) and the specific heat was measured by differential scanning calorimetry (Perkin Elmer, DSC 4000). Finally, the thermal conductivity κ was calculated from the individual properties according to following equation, where κ is the product of specific heat (C_p, J g^{-1} K^{-1}), density (ρ, g cm^{-3}), and thermal diffusivity (α, mm^2 s^{-1}).

$$\kappa = C_p \times \rho \times \alpha \quad (1)$$

Cooling Performance Measurement

The cooling performance was characterized in dependence of the applied strain using a homebuilt measuring system. A linear stage (Zaber tech. X-LHM-E) was used to apply the strain. The device was placed on top of the water block, which was used as a heat sink, and each end of the device was clamped in order to apply the strain. Temperatures were measured using thermocouples, which were connected to a multimeter (Keithley 2000). To test the cooling performance, one thermocouple was placed on top of the device located between the legs and another thermocouple was placed on the water block to measure the temperature decrease at the

top surface of the device. The temperatures were measured before and after the electric current was applied to the device by a power supply (Agilent, E3646A). The application of electrical current yields a decrease of the surface temperature due to the Peltier heat transport. Increasing the electric current flow causes a further decrease of the surface temperature until the maximum temperature drop is reached. Further increase of the electric current yield an increased impact of Joule heating, which lowers the temperature drop. The temperature drop was measured without strain and during stretching of the device up to 30%. For Ecoflex/alumina composite devices, the same process was done under different strains.

Applications

To demonstrate the cooling under heat load, the heat sink was fixed at 298 K during the experiment by using a bath circulator (JEIO TECH, RW3-2025). First, the Peltier module (Ferrotec, Peltier Cooler Model 9500/031/060B) was stacked between the Cu block and the heat sink without the stretchable TE cooling device. The heat load was supplied from a Cu block above the Peltier device and it was thermally powered with 0.8 W by Joule heating of a steel rod, which was inserted into the Cu block. To measure the temperature difference across the Peltier module, one thermocouple was placed on top of the heat sink, while another thermocouple was placed in a drilled hole at the center of the Cu block. After power was applied to the heat source (steel rod), the temperature of the block was monitored until it reached a steady state. It was assumed that the temperature of the top and bottom side of the Peltier module is represented by the temperature of the Cu block and the heat sink, respectively. The temperature difference across the Peltier module was later used for the conversion of output voltages into corresponding temperature values. Next,

the stretchable TE cooling device was stacked between the heat sink and the Peltier module for detection of thermal steady state conditions by means of its terminal voltage. Then, electric current was applied to the stretchable TE device after stabilization in order to measure the temperature drop by the activation of stretchable TE cooling device. The cooling performance was measured for changing levels of the applied strain up to 30%.

The surface temperature profile of the stretchable TE cooling device was additionally observed in another configuration using an IR camera. The device was placed on top of the heat sink, while hot air was directly blown onto the top side of the device by means of an electrical air blower. The temperature of the heat sink was fixed at 298 K and the top surface layer of the device was heated to ~316 K by the hot air. IR images were taken at the top surface of the device with and without application of electric current into the device, and the same process was done for 30% strain.

RESULTS AND DISCUSSION

Resistance Measurement

In Peltier modules, internal resistance R_{int} causes Joule heating that reduces its cooling performance.[66,67] Since R_{int} is an extensive property whose value changes with the dimensions of conductive paths, a deformation of a stretchable device under an external strain could result in varying R_{int} values in dependence of the applied strain. Thus, establishing the relation between R_{int} and the applied strain is of fundamental importance for a thorough and meaningful analysis of the cooling characteristics of a stretchable TE cooling device. We tested the change of R_{int} and its

repeatability on our stretchable cooling device by applying repeated cycles of 30% uniaxial strain and release (Figure 3a). R_{int} increased by 7% from 0.114 Ω to 0.122 Ω when the device was stretched by 30% and returned to the initial value of 0.114 Ω when the strain was released (Figure 3b). Such variation of R_{int} is attributed to the physical dimension changes of Galinstan channels during the stretching-and-releasing cycle. Assuming that the Galinstan electrodes have a rectangular shape with the width, height, and length of w_0, h_0, and l_0, respectively, the variation of R_{int} under strain can be estimated (see Supporting Information). As shown in Figure S3 the fabricated stretchable TE cooling device has electrical connections made by a combination of parallel and orthogonal Galinstan electrodes in relation to the direction of the applied strain. With the given direction of applied strain (Figure 3a), the increase of R_{int} is solely attributed to the simultaneous changes in the length and height of parallel electrodes. It is estimated that the R_{int} increases by 13% when a 30% strain is applied (see Supporting Information). The larger estimated increment in R_{int} than the experimentally measured 7% is possibly due to the assumption made on the shape of Galinstan electrodes. Since the number of parallel electrodes used in the stretchable TE cooling device largely affects the change of R_{int} under an applied strain, the electrical connection scheme has to be designed carefully for an optimized performance of stretchable TE cooling devices.

The simultaneous changes in the length and height of parallel electrodes are expected to lead to a non-linear dependence of R_{int} on the applied strain, which has been revealed by measuring R_{int} under a slowly varying strain with 0.05 mm/s (Figure 3c). The R_{int} shows a power of ~ 1.5 dependence on the applied strain while the calculated resistance shows a power of ~2 dependence (see Supporting Information). This difference could be explained by thinning of the electrodes under an applied strain for the region right above and under the TE legs. In this region, the electrical

path decreases and leads to a reducing effect of the R_{int}. Lastly, the 7% variation in R_{int} was repeatable over 1000 stretching-and-release cycles as shown in Figure 3d, revealing the mechanical resilience of the fabricated device.

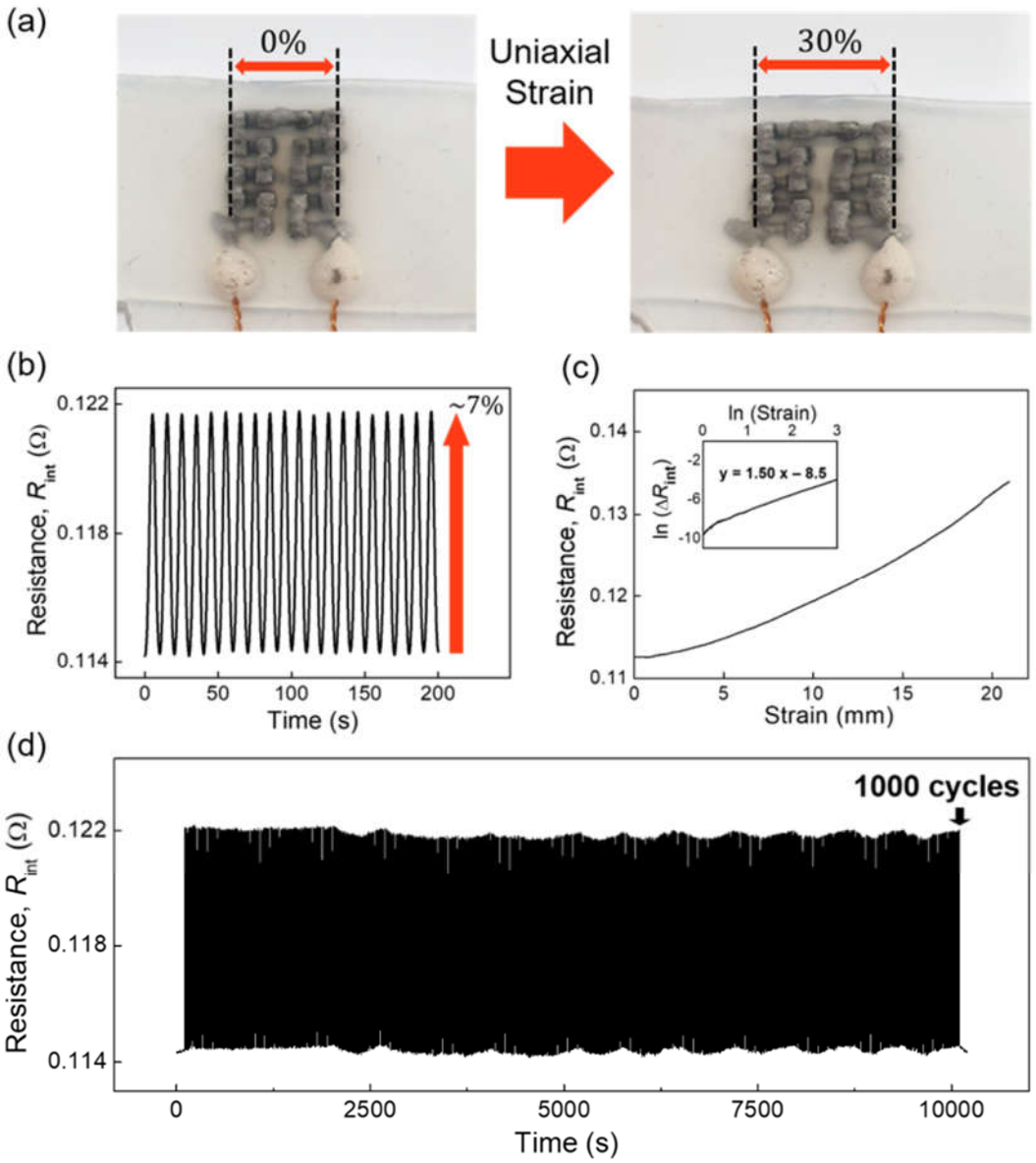

Figure 3. Internal resistance measurements of stretchable thermoelectric cooling device. (a) Photographs of the device uniaxially stretched by applied 30% strain. (b) Changes of internal resistance, R_{int}, during repeated stretching and releasing cycles. (c) Dependency between the

internal resistance and strain. Inset shows the power law dependence of R_{int} on the applied strain. (d) The resistance was measured during 1000 cycles to test device resilience.

Cooling Performance under Zero Heat Load

First, the cooling performance with no external heat load was measured under different applied strains. The initial device (Figure 4a, left) was fabricated using pure Ecoflex for the substrates. κ of pure Ecoflex was measured to be 0.27 $W \cdot m^{-1} \cdot K^{-1}$ at 300 K as shown in Figure 4b (see Experimental Section for details). A thermal circuit analysis reveals that using this poor thermal conductor as the top and bottom substrates introduces high thermal resistances to the whole device, significantly degrading its cooling performance (see Figure S4 in Supporting Information). The same issue can happen in any stretchable or flexible cooling devices that employ polymers in their structures. The calculated result shows that improving κ of the top and bottom substrates can substantially enhance the device's cooling performance. As one way to increase the κ of Ecoflex at the top and bottom substrates, we introduced alumina powder as a filler material into the Ecoflex due to its high κ (~ 30 $W \cdot m^{-1} K^{-1}$ at 300 K),[68] electrically insulating property, and low cost compared to other ceramic fillers, such as boron nitride.[69] The composites were fabricated by mixing Ecoflex with 0, 20, 40, or 60 wt. % of alumina powder (herein called D00, D20, D40, and D60, respectively), and all of D00, D20, D40, and D60 showed excellent mechanical robustness in stress-strain tests up to 440% strain (Figure S5a). The stiffest sample with the highest alumina concentration, D60, was additionally tested to check its mechanical endurance over 1000 stretching-and-releasing cycles up to 30% strain. As shown in Figure S5b, it demonstrates stable stress-strain behavior over the entire cycles. The Ecoflex/alumina composites show improved κ

from 0.27 $W \cdot m^{-1} \cdot K^{-1}$ in D00 to 0.37, 0.54, 0.81 $W\ m^{-1}\ K^{-1}$ in D20, D40, and D60, respectively (Figure 4b). The distribution of the alumina powder was observed using scanning electron microscope (SEM) and back scattered electron (BSE) images (Figure S1). The disproportional increase in κ with alumina concentration could be caused by a formation of thermally-conductive alumina channels.[24,25] The devices fabricated with Ecoflex/alumina composites with a high alumina concentration exhibit opaque surfaces as shown in Figure 4a (right).

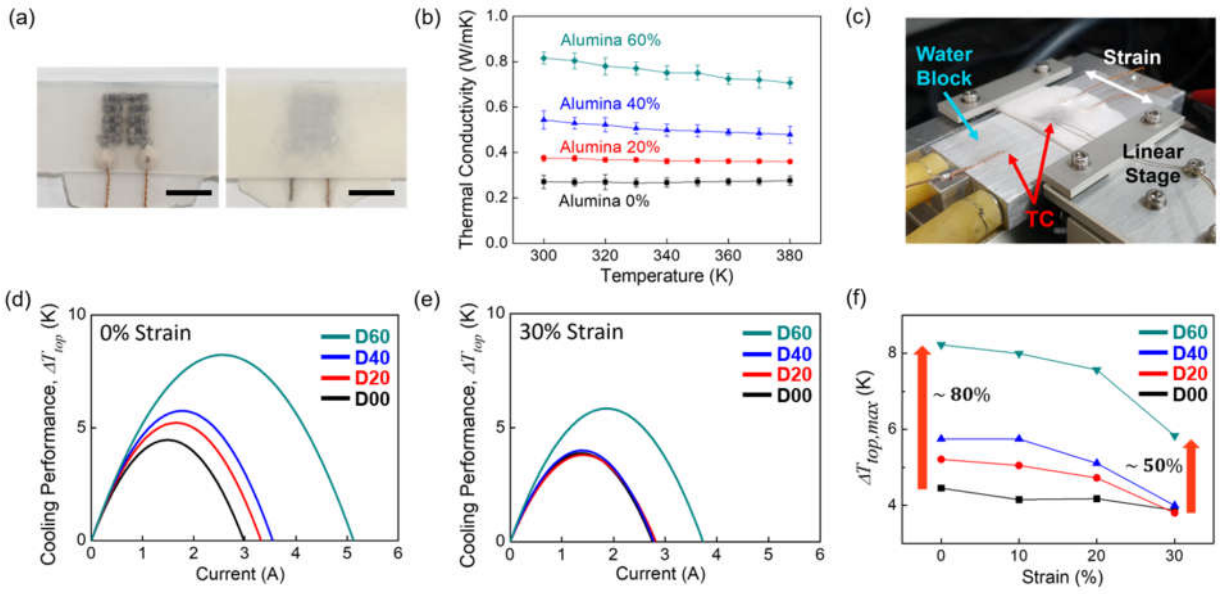

Figure 4. Characterization of cooling performance with no external heat load. (a) Stretchable thermoelectric cooling device without alumina powder (left) and with 60% alumina powder (right). Scale bars: 10 mm. (b) Thermal conductivity measurements of Ecoflex/alumina composites with different alumina concentrations. (c) Experimental setup for measuring the cooling performance without heat load. ΔT_{top} is the temperature drop at the top layers of the device. ΔT_{top} for each of the devices was measured (d) at 0% strain and (e) at 30% strain with varying electrical current

inputs to the devices. (f) Dependence of the maximum temperature drop, $\Delta T_{top,max}$, on the applied strain.

For characterization of the cooling performance, thermocouples were attached on the heat sink (water block) and the top surface of each device (Figure 4c) to monitor the temperature variation. ΔT_{top}, the temperature drop at the top surface of the device, was monitored as the electrical current applied to the device was varied. The temperature on the top of the heat sink was maintained at ~ 293 K throughout the measurements. In general, at low currents, the Peltier cooling effect remains dominant until the ΔT_{top} reaches its maximum. ΔT_{top} starts to decrease for larger currents as Joule heating becomes more dominant (Figure 4d and 4e). ΔT_{top} was measured with applied strains up to 30% for all devices with different alumina concentrations. At every strain value, the devices with larger alumina concentrations show better cooling performance as shown in Figure 4d, 4e, and Figure S6, qualitatively consistent with the theoretical calculation results (Figure S4). This proves that the reduction of the thermal resistance in the top and bottom substrates indeed improves the cooling performance of stretchable TE cooling devices. At 0% strain, the maximum ΔT_{top} for each tested substrate is 4.5 K, 5.2 K, 5.7 K, and 8.2 K for D00, D20, D40, and D60, respectively (Figure 4d). At 30% strain, the maximum ΔT_{top} is 3.8 K, 3.8 K, 4.0 K, and 5.8 K for D00, D20, D40, and D60, respectively (Figure 4e). The percolation threshold, which is known from dielectrics to describe a long-range connectivity of conductive particles inside non-conductive matrices, can explain the significant increase in ΔT_{top} for the device with 60 wt. % alumina (D60). The alumina particles form thermally conductive paths inside the Ecoflex substrate, which yield the rapid increase of heat conduction, effectively decreasing the thermal transfer resistance of the substrate. This hypothesis is supported by the aforementioned disproportional

increase in κ with alumina concentration (Figure 4b). It is also noted that the electrical current required to achieve the maximum ΔT_{top}, $I_{\max}$, increases as the alumina concentration increases. The $I_{\max}$ occurs as a result of competition between the removed heat flow from the top surface and the reverse heat flow by Joule heating at a given I. As I further increases, Joule heating becomes more dominant, which leads to the decrease of ΔT_{top}. Now, as the thermal conductance of the Ecoflex layers increases with increasing alumina concentration, a larger heat flow can be drawn by the device for a given I. This leads to the delayed occurrence of $I_{\max}$ at a larger I value and explains the experimentally observed trend.

In order to examine the dependence of cooling performance on the applied strain, $\Delta T_{top,max}$, the maximum temperature drop at the top surface, is plotted as a function of the applied strain (Figure 4f). All devices show a qualitatively similar behavior where $\Delta T_{top,max}$ decreases with increasing strain. The result is consistent with the observation that the internal electrical resistance of all devices increases as the applied strain increases (Figure S7). It is noted that the decreasing rate of $\Delta T_{top,max}$ with strain is much higher for the devices with higher alumina concentrations, resulting in the almost same $\Delta T_{top,max}$ for D00, D20, and D40 when 30% strain is applied. This also leads to the relatively small improvement (~ 50%) in $\Delta T_{top,max}$ when 60 wt. % alumina is added, compared to the ~ 80% improvement at zero strain. The disproportionately decreasing rates of $\Delta T_{top,max}$ depending on the alumina concentration can be explained by considering the simultaneous changes of R_{int} and the thermal conductance of each device under strain. Here, the thermal conductance of each device means the thermal conductance across the device thickness (height). While the increasing rates of R_{int} with strain are similar for the four devices (Figure S7), changes of thermal conductance are estimated to be different between the devices due to the following reason. Depending on the alumina concentration, the top and bottom substrates of each device

have different stiffness; those with the higher alumina concentrations are stiffer. Assuming that the height of TE legs and thermal contact resistances between different layers do not change under strain, the change of thermal conductance across each device is mainly determined by the thickness change of the top and bottom substrates. Generally, stretching reduces the thickness of the substrates, and thus increases the thermal conductance across these layers. As for the relation to the cooling performance ΔT_{top}, increasing the thermal conductance of substrates leads to a larger ΔT_{top}, whereas increasing the R_{int} does the opposite. Since the stiffer substrates with higher alumina concentrations suffer a smaller thickness decrease under the same strain, the accompanied increase of thermal conductance remains relatively smaller. Combined with the similar increasing rates of R_{int} under strain, this smaller increase rates of the thermal substrate conductance in devices with higher alumina concentrations result in the observed faster decreasing rate of $\Delta T_{top,max}$ with increasing strain (Figure 4f).

Our stretchable cooling devices show much smaller $\Delta T_{top,max}$ (4 ~ 8 K) compared to that of the commercial Peltier module (~ 60 K, see Figure S8 in the Supporting Information) from which the TE legs were extracted. The discrepancy can be qualitatively explained by multiple factors, such as less optimized electrical and thermal contacts, large thermal resistances of the Ecoflex substrates even with the introduction of alumina powder, and heat loss through the Ecoflex fillers in-between TE legs in the stretchable devices. Such considerations need to be addressed to further improve the cooling performance of stretchable TE cooling devices.

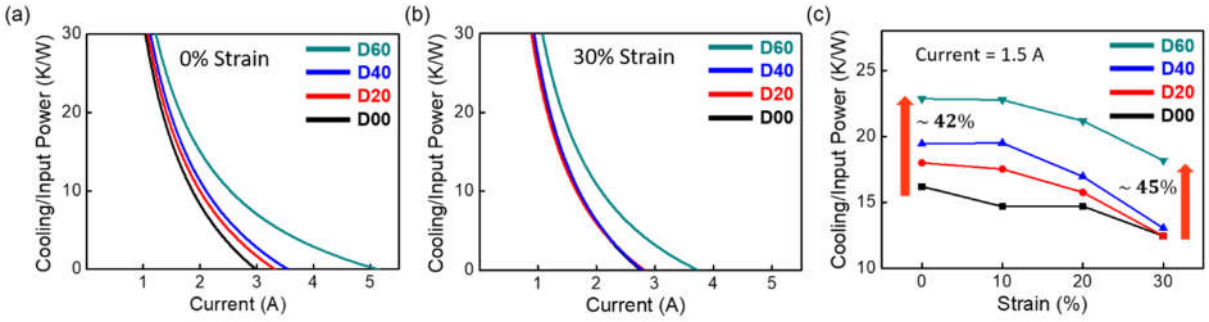

Figure 5. Magnitude of temperature reduction over input electric power for the stretchable thermoelectric cooling device (a) at 0% strain and (b) at 30% strain with varying electrical current inputs to the devices. D60 shows the highest cooling per input power at a fixed current, followed by the D40, D20, and D00. (c) Dependence of the cooling efficiency on the applied strain at a fixed electrical current input of 1.5 A to the devices.

For cost-benefit analysis,[70] we plot the amount of cooling per applied electrical power as a function of applied electrical current (Figure 5a and 5b). At a fixed current, the cooling per input power is higher for the devices with higher alumina concentrations, which means relatively less electrical power is required for those devices to perform the same amount of cooling. For instance, at a fixed electrical current input of 1.5 A, D60 shows the highest cooling per input electric power at strains up to 30% followed by D40, D20, and D00 (Figure 5c and S9). The cooling per input power of D60 is higher than that of D00 by 42% and 45% at 0% and 30% strains, respectively. All devices show decreasing cooling per input power as strain increases, similar to the trend observed for $\Delta T_{top,max}$ versus strain (Figure 4f).

Cooling Performance under Heat Load

A stretchable TE cooling device can be applied for thermal management of flexible or stretchable electronic devices. These devices could generate a considerable amount of heat, which can affect the operating performance of the cooling device due to variations of the effective temperature, and thereby degrade its cooling curve. Therefore, the cooling performance of the fabricated stretchable TE cooling device was evaluated under different heat load conditions (Figure 6). Among the fabricated devices, D60, the best performing device from the precedent no heat load experiment, was used to demonstrate cooling under heat load conditions. The external heat was applied using each of conduction (Figure 6a and 6b) and convection (Figure 6c-e).

First, conductive heating was supplied by a Cu block heater, which generated the constant heat load of 0.8 W throughout the measurements. The induced strain on the device, due to the pressure applied by the Cu block, is calculated to be an order of magnitude smaller than the applied strain values in our experiments; rather, the weight of the Cu block provides better thermal contacts between the constituent layers in the experimental setup. The cooling performance of D60 was evaluated by monitoring the temperature drop at the top surface of the device (ΔT_{top}) using a Peltier module (Figure 6a). The Peltier module provides better thermal contacts between the adjacent surfaces as well as more representative temperature readings of the entire top surface of D60 than those provided by conventional thermocouples. The output voltage of the Peltier module can be converted into temperature scale by calibrating it with the measured temperature values by the thermocouples attached to the heater and the top of the heat sink. The measured maximum temperature drop ΔT_{top} = 1.65 K, 1.43 K, 1.39 K, 1.31 K at 0%, 10%, 20%, and 30% strains, respectively (Figure 6b), smaller than $\Delta T_{top,max}$ reported under no heat load condition. Without

external heat load, only half of the internal losses due to Joule heat generation is transported from the cold to the hot side of the cooling device, yielding the maximum temperature drop reported in Figure 4f. $\Delta T_{top,max}$ of the cooling device decreases when a heat load is applied, since fractions of the externally applied heat have to be transported additionally to the half of the internal Joule heat generation.

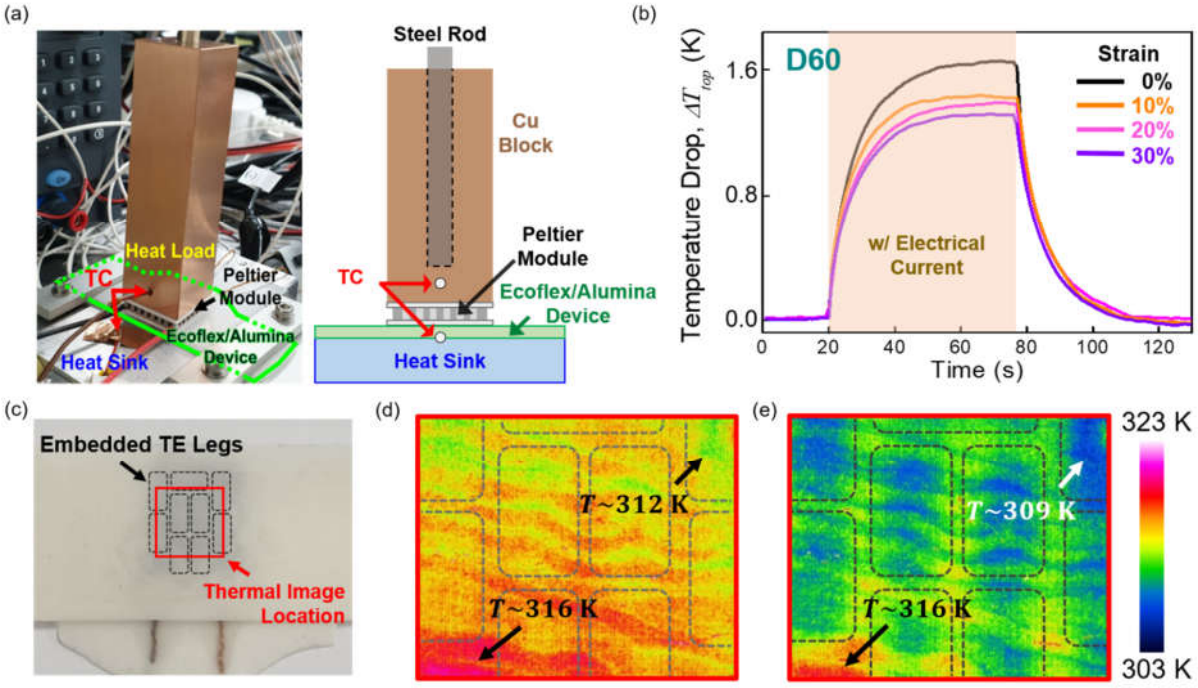

Figure 6. Cooling performance of 60 wt. % Ecoflex/alumina device (D60) under conductive heat load (a,b) and convective heat load (c-e). (a) Experiment setup, schematic diagram of the experiment, and (b) ΔT_{top}, the temperature drop at the interface between the stretchable TE device and the Peltier module under the constant conduction heat load of 0.8 W from the Cu block. The data was obtained 20 s after application of the electrical current for strains up to 30%. (c) Photograph image of the 60 wt. % Ecoflex/alumina device. (d) Thermal images were taken while applying hot air over the top layer of the device, and (e) during active cooling with applied electrical current.

For the convective heating experiment, a linear stage, water block and the stretchable TE cooling device were placed below an infrared (IR) camera (Figure S10a) and heat was provided using a hot air blower. The temperature scale of the IR camera was calibrated for D60 by comparing the output voltage of the IR camera to the thermocouple reading on the device surface, which addresses the emissivity of the device. D60 showed an emissivity of 0.53. First, D60 was placed on top of the water block. The dashed-boundary lines in Figure 6c indicate the location of the TE legs embedded inside the device. Then hot air was blown at the top surface of the device and the IR camera was used to observe the temperature profile of the surface. While the surface temperature reaches 316 K at steady state on the peripheral area, the temperature is 312 K in the areas wherein the TE legs are embedded (Figure 6d). The temperature drop is caused by heat conduction through the TE legs towards the bottom side of the device, which is held at 298 K by the water block heat sink. The wave pattern in the IR image is due to inhomogeneity of the sample substrate caused by agglomeration of alumina particles inside Ecoflex during the fabrication. When the same 1.8 A of electric current as in the case of conductive heating was applied to the device, the TE cooling device initiated its active cooling, yielding a temperature reduction at the locations of TE legs from 312 K to 309 K (Figure 6e). To examine the effect of strain, the surface temperature profiles of D60 at strains of 0% and 30% were observed using the IR camera under convective heat load (Figure S10b and Video S1). The observed surface temperature during the active cooling increases from 309 K to 310.7 K when the applied strain increases from 0% to 30%, which again could be attributed to an increased R_{int} under strain. It is noted that a larger temperature drop at the top surface of each device is observed under the convective heat load conditions than under the conductive heat load conditions. A quantitative explanation of the observed discrepancy requires further detailed information such as the difference in the heat load, thermal capacitances

and contact resistances between the two experimental systems, which are not available in the current work.

CONCLUSIONS

In this work, a stretchable TE cooling device is fabricated by embedding Bi-Te-based TE legs and Galinstan in a stretchable Ecoflex substrate. Our stretchable TE devices not only feature a relatively simple design and a low-cost fabrication process, but also show excellent mechanical robustness against 1000 cycles of stretching-and-releasing without any observable functional degradation. Regarding the cooling performance of the stretchable TE devices, the poor thermal conductivity of Ecoflex substrates imposes considerable thermal resistances to the entire device, significantly degrading the cooling capability. The issue is addressed by introducing alumina powder into the Ecoflex substrates, which largely improves the thermal conductivity while maintaining reasonable stretchability. As a result, the maximum temperature drop at 0% strain reaches 8.2 K when 60 wt. % of alumina is used, which corresponds to 80% improvement compared to the case where no alumina is used. While applying 30% strain reduces the maximum temperature drop to 5.8 K, it still represents about 50% improvement over the no alumina case. Furthermore, the devices with higher alumina concentrations show considerable improvement in cooling per input electrical power, suggesting their merit in cost and energy saving. Considering that many stretchable devices employ stretchable polymers, which are generally poor thermal conductors, our study underscores the importance of improving their thermal conductivity from the viewpoint of cooling and provides an effective way to do so. Finally, cooling tests under conductive and convective heat load conditions demonstrate the potential of the fabricated stretchable TE devices for real applications such as wearable electronics and thermal sensing devices.

ASSOCIATED CONTENT

Supporting Information.

Supporting Video shows IR images on the top surface of the 60 wt. % Ecoflex/alumina device at 0% and 30% strain while applying convective heat (MP4). The temperature scale matches that used in Figure 6d and e. The increase of temperature at the later part is due to overtaking of Joule heating effect.

Supporting Information contains the following content: SEM and BSE images of Ecoflex/alumina composites; thermal property measurements of 0, 20, 40, 60 wt. % Ecoflex/alumina; calculation of the internal resistance at strain of 30%; power law calculation of the internal resistance; schematic diagram and thermal circuit model for the device; theoretical calculation of the cooling performance with changes in thermal conductivity; mechanical property measurements of 0, 20, 40, 60 wt. % Ecoflex/alumina; mechanical endurance measurement during 1000 cycle of the 60 wt. % Ecoflex/alumina device at 30% strain; temperature drop at the top surface of the devices; internal resistance measurement for each composite device; cooling performance measurement of the commercial Peltier device; cooling temperature over input power for each device; IR images of the device at 0 and 30% strain during application of current (PDF)

AUTHOR INFORMATION

Corresponding Author

*E-mail: hgjin@postech.ac.kr

Author Contributions

All of the authors read and approved the final version of the manuscript.

Notes

The authors declare no competing financial interest.

ACKNOWLEDGMENT

The authors would like to thank Prof. Un-yong Jeong for help with the mechanical property measurement. This work was supported by the National Research Foundation of Korea (NRF) grant funded by the Korea government (MSIT) (NRF-2020R1C1C1004291), and by the Korea Institute of Energy Technology Evaluation and Planning (KETEP) grant funded by the Korea government (MOTIE) (20188550000290, Development of Meta-Silicide Thermoelectric Semiconductor and Metrology Standardization Technology of Thermoelectric Power module)

REFERENCES

(1) Bao, Z.; Chen, X. Flexible and Stretchable Devices. *Adv. Mater.* **2016**, *28* (22), 4177–4179.

(2) Hammock, M. L.; Chortos, A.; Tee, B. C. K.; Tok, J. B. H.; Bao, Z. 25th Anniversary Article: The Evolution of Electronic Skin (E-Skin): A Brief History, Design Considerations, and Recent Progress. *Adv. Mater.* **2013**, *25* (42), 5997–6038.

(3) Rogers, J. A.; Someya, T.; Huang, Y.; Sorensen, A. E.; Lian, J.; Greer, J. R.; Valdevit, L.; Carter, W. B.; Ge, Q.; Jackson, J. A.; Kucheyev, S. O.; Fang, N. X.; Spadaccini, C. M. Materials and Mechanics for Stretchable Electronics. *Science (80-.).* **2010**, *327* (5973), 1603–1607.

(4) Kim, D.-H.; Ghaffari, R.; Lu, N.; Rogers, J. A. Flexible and Stretchable Electronics for Biointegrated Devices. *Annu. Rev. Biomed. Eng.* **2012**, *14* (1), 113–128.

(5) Kim, D. H.; Rogers, J. A. Stretchable Electronics: Materials Strategies and Devices. *Adv. Mater.* **2008**, *20* (24), 4887–4892.

(6) Wu, H.; Huang, Y. A.; Xu, F.; Duan, Y.; Yin, Z. Energy Harvesters for Wearable and Stretchable Electronics: From Flexibility to Stretchability. *Adv. Mater.* **2016**, *28* (45), 9881–9919.

(7) Song, H.; Liu, J.; Liu, B.; Wu, J.; Cheng, H. M.; Kang, F. Two-Dimensional Materials for Thermal Management Applications. *Joule* **2018**, *2* (3), 442–463.

(8) Hamann, H. F.; Weger, A.; Lacey, J. A.; Hu, Z.; Bose, P.; Cohen, E.; Wakil, J. Hotspot-Limited Microprocessors: Direct Temperature and Power Distribution Measurements. *IEEE J. Solid-State Circuits* **2007**, *42* (1), 56–64.

(9) Tan, C.; Zhu, H.; Ma, T.; Guo, W.; Liu, X.; Huang, X.; Zhao, H.; Long, Y-Z.; Jiang, P.; Sun, B. A Stretchable laminated GNRs/BNNSs nanocomposite with high electrical and thermal conductivity. *Nanoscale* **2019,** *11* (43), 20648-20658.

(10) Zabrocki, K.; Goupil, C.; Ouerdane, H.; Apertet, Y.; Seifert, W.; Eckhard, M. Continuum Theory and Modeling of Thermoelectric Elements (Ed: C. Goupil), Wiley-VCH, Berlin, Germany **2016**, 1–74.

(11) Enescu, D.; Virjoghe, E. O. A Review on Thermoelectric Cooling Parameters and Performance. *Renew. Sustain. Energy Rev.* **2014**, *38*, 903–916.

(12) Anant Kishore, R.; Kumar, P.; Sanghadasa, M.; Priya, S. Taguchi optimization of Bismuth-Telluride based thermoelectric cooler. *J. Appl. Phys.* **2017**, *122*, 025109.

(13) Sharma, S.; Dwivedi, V.; Pandit, S. A review of thermoelectric devices for cooling applications. *Int. J. Green Energy* **2014**, *11*, 899–909.

(14) Laser Electronics. Heat Sink Cool 30. https://laser-electronics.de/Cool30.htm. Accessed January 12, 2021.

(15) Chowdhury, I.; Prasher, R.; Lofgreen, K.; Chrysler, G.; Narasimhan, S.; Mahajan, R.; Koester, D.; Alley, R.; Venkatasubramanian, R. On-Chip Cooling by Superlattice-Based Thin-Film Thermoelectrics. *Nat. Nanotechnol.* **2009**, *4* (4), 235–238.

(16) Bulman, G.; Barletta, P.; Lewis, J.; Baldasaro, N.; Manno, M.; Bar-Cohen, A.; Yang, B. Superlattice-Based Thin-Film Thermoelectric Modules with High Cooling Fluxes. *Nat. Commun.* **2016**, *7*, 1–7.

(17) Zebarjadi, M. Electronic Cooling Using Thermoelectric Devices. *Appl. Phys. Lett.* **2015**, *106* (20), 203506.

(18) Zhu, B.; Liu, J.; Wang, T.; Han, M.; Valloppilly, S.; Xu, S.; Wang, X. Novel Polyethylene Fibers of Very High Thermal Conductivity Enabled by Amorphous Restructuring. *ACS Omega* **2017**, *2* (7), 3931–3944.

(19) Chen, H.; Ginzburg, V. V.; Yang, J.; Yang, Y.; Liu, W.; Huang, Y.; Du, L.; Chen, B. Thermal Conductivity of Polymer-Based Composites: Fundamentals and Applications. *Prog. Polym. Sci.* **2016**, *59*, 41–85.

(20) Burger, N.; Laachachi, A.; Ferriol, M.; Lutz, M.; Toniazzo, V.; Ruch, D. Review of Thermal Conductivity in Composites: Mechanisms, Parameters and Theory. *Prog. Polym. Sci.* **2016**, *61*, 1–28.

(21) Kang, S.; Kang, T. H.; Kim, B. S.; Oh, J.; Park, S.; Choi, I. S.; Lee, J.; Son, J. G. 2D Reentrant Micro-Honeycomb Structure of Graphene-CNT in Polyurethane: High Stretchability, Superior Electrical/Thermal Conductivity, and Improved Shape Memory Properties. *Compos. Part B Eng.* **2019**, *162*, 580–588.

(22) Song, J.; Chen, C.; Zhang, Y. High Thermal Conductivity and Stretchability of Layer-by-Layer Assembled Silicone Rubber/Graphene Nanosheets Multilayered Films. *Compos. Part A Appl. Sci. Manuf.* **2018**, *105*, 1–8.

(23) Pan, G.; Yao, Y.; Zeng, X.; Sun, J.; Hu, J.; Sun, R.; Xu, J. Bin; Wong, C. P. Learning from Natural Nacre: Constructing Layered Polymer Composites with High Thermal Conductivity. *ACS Appl. Mater. Interfaces* **2017**, *9* (38), 33001–33010.

(24) Wu, Y.; Ye, K.; Liu, Z.; Wang, M.; Chee, K. W. A.; Lin, C. Te; Jiang, N.; Yu, J. Effective Thermal Transport Highway Construction within Dielectric Polymer Composites: Via a Vacuum-Assisted Infiltration Method. *J. Mater. Chem. C* **2018**, *6* (24), 6494–6501.

(25) Zhou, W.; Wang, C.; An, Q.; Ou, H. Thermal Properties of Heat Conductive Silicone Rubber Filled with Hybrid Fillers. *J. Compos. Mater.* **2008**, *42* (2), 173–187.

(26) Hong, H.; Jung, Y. H.; Lee, J. S.; Jeong, C.; Kim, J. U.; Lee, S.; Ryu, H.; Kim, H.; Ma, Z.; Kim, T. il. Anisotropic Thermal Conductive Composite by the Guided Assembly of Boron Nitride Nanosheets for Flexible and Stretchable Electronics. *Adv. Funct. Mater.* **2019**, *1902575*, 1–10.

(27) Kwon, O. H.; Ha, T.; Kim, D. G.; Kim, B. G.; Kim, Y. S.; Shin, T. J.; Koh, W. G.; Lim, H. S.; Yoo, Y. Anisotropy-Driven High Thermal Conductivity in Stretchable Poly(Vinyl Alcohol)/Hexagonal Boron Nitride Nanohybrid Films. *ACS Appl. Mater. Interfaces* **2018**, *10*, 34625–34633.

(28) Jeong, S. H.; Chen, S.; Huo, J.; Gamstedt, E. K.; Liu, J.; Zhang, S. L.; Zhang, Z. Bin; Hjort, K.; Wu, Z. Mechanically Stretchable and Electrically Insulating Thermal Elastomer Composite by Liquid Alloy Droplet Embedment. *Sci. Rep.* **2015**, *5*, 1–10.

(29) Wang, J.; Cai, G.; Li, S.; Gao, D.; Xiong, J.; Lee, P. S. Printable Superelastic Conductors with Extreme Stretchability and Robust Cycling Endurance Enabled by Liquid-Metal Particles. *Adv. Mater.* **2018**, *30* (16), 24–26.

(30) Dickey, M. D. Stretchable and Soft Electronics Using Liquid Metals. *Adv. Mater.* **2017**, *29* (27), 592–601.

(31) Park, S. H.; Jo, S.; Kwon, B.; Kim, F.; Ban, H. W.; Lee, J. E.; Gu, D. H.; Lee, S. H.; Hwang, Y.; Kim, J. S.; Hyun, D. Bin; Lee, S.; Choi, K. J.; Jo, W.; Son, J. S. High-Performance Shape-Engineerable Thermoelectric Painting. *Nat. Commun.* **2016**, *7*, 1–10.

(32) Kim, S. J.; We, J. H.; Cho, B. J. A Wearable Thermoelectric Generator Fabricated on a Glass Fabric. *Energy Environ. Sci.* **2014**, *7* (6), 1959–1965.

(33) Chen, Y.; Zhao, Y.; Liang, Z. Solution Processed Organic Thermoelectrics: Towards Flexible Thermoelectric Modules. *Energy Environ. Sci.* **2015**, *8* (2), 401–422.

(34) Wu, H.; Huang, Y. A.; Xu, F.; Duan, Y.; Yin, Z. Energy Harvesters for Wearable and Stretchable Electronics: From Flexibility to Stretchability. *Adv. Mater.* **2016**, *28* (45), 9881–9919.

(35) Yadav, A.; Pipe, K. P.; Shtein, M. Fiber-Based Flexible Thermoelectric Power Generator. *J. Power Sources* **2008**, *175* (2), 909–913.

(36) Siddique, A. R. M.; Mahmud, S.; Heyst, B. Van. A Review of the State of the Science on Wearable Thermoelectric Power Generators (TEGs) and Their Existing Challenges. *Renew. Sustain. Energy Rev.* **2017**, *73*, 730–744.

(37) Lu, Z.; Zhang, H.; Mao, C.; Li, C. M. Silk Fabric-Based Wearable Thermoelectric Generator for Energy Harvesting from the Human Body. *Appl. Energy* **2016**, *164*, 57–63.

(38) Suarez, F.; Parekh, D. P.; Ladd, C.; Vashaee, D.; Dickey, M. D.; Öztürk, M. C. Flexible Thermoelectric Generator Using Bulk Legs and Liquid Metal Interconnects for Wearable Electronics. *Appl. Energy* **2017**, *202*, 736–745.

(39) Du, Y.; Xu, J.; Paul, B.; Eklund, P. Flexible Thermoelectric Materials and Devices. *Appl. Mater. Today* **2018**, *12*, 366–388.

(40) Yang, C.; Souchay, D.; Kneiß, M.; Bogner, M.; Wei, H. M.; Lorenz, M.; Oeckler, O.; Benstetter, G.; Fu, Y. Q.; Grundmann, M. Transparent Flexible Thermoelectric Material Based on Non-Toxic Earth-Abundant p-Type Copper Iodide Thin Film. *Nat. Commun.* **2017**, *8*, 4–10.

(41) Goncalves, L. M.; Rocha, J. G.; Couto, C.; Alpuim, P.; Min, G.; Rowe, D. M.; Correia, J. H. Fabrication of Flexible Thermoelectric Microcoolers Using Planar Thin-Film Technologies. *J. Micromech. Microeng.* **2007**, *17* (7), S168-S173.

(42) Madan, D.; Wang, Z.; Wright, P. K.; Evans, J. W. Printed Flexible Thermoelectric Generators for Use on Low Levels of Waste Heat. *Appl. Energy* **2015**, *156*, 587–592.

(43) Lee, J. A.; Aliev, A. E.; Bykova, J. S.; de Andrade, M. J.; Kim, D.; Sim, H. J.; Lepró, X.; Zakhidov, A. A.; Lee, J. B.; Spinks, G. M.; Roth, S.; Kim, S. J.; Baughman, R. H. Woven-Yarn Thermoelectric Textiles. *Adv. Mater.* **2016**, *28* (25), 5038–5044.

(44) Zhou, C.; Dun, C.; Wang, Q.; Wang, K.; Shi, Z.; Carroll, D. L.; Liu, G.; Qiao, G. Nanowires as Building Blocks to Fabricate Flexible Thermoelectric Fabric: The Case of Copper Telluride Nanowires. *ACS Appl. Mater. Interfaces* **2015**, *7* (38), 21015–21020.

(45) Sevilla, G. A. T.; Inayat, S. Bin; Rojas, J. P.; Hussain, A. M.; Hussain, M. M. Flexible and Semi-Transparent Thermoelectric Energy Harvesters from Low Cost Bulk Silicon (100). *Small* **2013**, *9* (23), 3916–3921.

(46) Francioso, L.; De Pascali, C.; Farella, I.; Martucci, C.; Cretì, P.; Siciliano, P.; Perrone, A. Flexible Thermoelectric Generator for Wearable Biometric Sensors. *Proc. IEEE Sensors* **2010**, 747–750.

(47) Kim, C. S.; Lee, G. S.; Choi, H.; Kim, Y. J.; Yang, H. M.; Lim, S. H.; Lee, S. G.; Cho, B. J. Structural Design of a Flexible Thermoelectric Power Generator for Wearable Applications. *Appl. Energy* **2018**, *214*, 131–138.

(48) Wang, Y.; Yang, L.; Shi, X. L.; Shi, X.; Chen, L.; Dargusch, M. S.; Zou, J.; Chen, Z. G. Flexible Thermoelectric Materials and Generators: Challenges and Innovations. *Adv. Mater.* **2019**, *31* (29), 1–47.

(49) Siddique, A. R. M.; Rabari, R.; Mahmud, S.; Heyst, B. Van. Thermal Energy Harvesting from the Human Body Using Flexible Thermoelectric Generator (FTEG) Fabricated by a Dispenser Printing Technique. *Energy* **2016**, *115*, 1081–1091.

(50) Wang, L.; Zhang, Z.; Geng, L.; Yuan, T.; Liu, Y.; Guo, J.; Fang, L.; Qiu, J.; Wang, S. Solution-Printable Fullerene/TiS2 Organic/Inorganic Hybrids for High-Performance Flexible n-Type Thermoelectrics. *Energy Environ. Sci.* **2018**, *11* (5), 1307–1317.

(51) Nguyen Huu, T.; Nguyen Van, T.; Takahito, O. Flexible Thermoelectric Power Generator with Y-Type Structure Using Electrochemical Deposition Process. *Appl. Energy* **2018**, *210*, 467–476.

(52) Hong, S.; Gu, Y.; Seo, J. K.; Wang, J.; Liu, P.; Shirley Meng, Y.; Xu, S.; Chen, R. Wearable Thermoelectrics for Personalized Thermoregulation. *Sci. Adv.* **2019**, *5*, eaaw0536.

(53) Malakooti, M. H.; Kazem, N.; Yan, J.; Pan, C.; Markvicka, E. J.; Matyjaszewski, K.; Majidi, C. Liquid Metal Supercooling for Low-Temperature Thermoelectric Wearables. *Adv. Funct. Mater.* **2019**, *29* (45), 1–9.

(54) Nan, K.; Kang, S. D.; Li, K.; Yu, K. J.; Zhu, F.; Wang, J.; Dunn, A. C.; Zhou, C.; Xie, Z.; Agne, M. T.; Wang, H.; Luan, H.; Zhang, Y.; Huang, Y.; Snyder, G. J.; Rogers, J. A. Compliant and Stretchable Thermoelectric Coils for Energy Harvesting in Miniature Flexible Devices. *Sci. Adv.* **2018**, *4* (11), 1–8.

(55) Rojas, J. P.; Singh, D.; Conchouso, D.; Arevalo, A.; Foulds, I. G.; Hussain, M. M. Stretchable Helical Architecture Inorganic-Organic Hetero Thermoelectric Generator. *Nano Energy* **2016**, *30*, 691–699.

(56) Jeong, S. H.; Cruz, F. J.; Chen, S.; Gravier, L.; Liu, J.; Wu, Z.; Hjort, K.; Zhang, S. L.; Zhang, Z. Bin. Stretchable Thermoelectric Generators Metallized with Liquid Alloy. *ACS Appl. Mater. Interfaces* **2017**, *9* (18), 15791–15797.

(57) Xu, X.; Zuo, Y.; Cai, S.; Tao, X.; Zhang, Z.; Zhou, X.; He, S.; Fang, X.; Peng, H. Three-Dimensional Helical Inorganic Thermoelectric Generators and Photodetectors for Stretchable and Wearable Electronic Devices. *J. Mater. Chem. C* **2018**, *6* (18), 4866–4872.

(58) Fukuie, K.; Iwata, Y.; Iwase, E. Design of Substrate Stretchability Using Origami-like Folding Deformation for Flexible Thermoelectric Generator. *Micromachines* **2018**, *9* (7), 315.

(59) Kim, J. Y.; Oh, J. Y.; Lee, T. Il. Multi-Dimensional Nanocomposites for Stretchable Thermoelectric Applications. *Appl. Phys. Lett.* **2019**, *114* (4), 043902.

(60) Zadan, M.; Malakooti, M. H.; Majidi, C. Soft and Stretchable Thermoelectric Generators Enabled by Liquid Metal Elastomer Composites. *ACS Appl. Mater. Interfaces* **2020**, *12* (15), 17921–17928.

(61) Lee, J.; Sul, H.; Lee, W.; Pyun, K. R.; Ha, I.; Kim, D.; Park, H.; Eom, H.; Yoon, Y.; Jung, J.; Lee, D.; Ko, S. H. Stretchable Skin-Like Cooling/Heating Device for Reconstruction of Artificial Thermal Sensation in Virtual Reality. *Adv. Funct. Mater.* **2020**, *30* (29), 1–11.

(62) Eom, S.; Lim, S. Stretchable Complementary Split Ring Resonator (CSRR)-Based Radio Frequency (RF) Sensor for Strain Direction and Level Detection. *Sensors* **2016**, *16* (10), 1–12.

(63) Hodes, M.; Zhang, R.; Lam, L. S.; Wilcoxon, R.; Lower, N. On the Potential of Galinstan-Based Minichannel and Minigap Cooling. *IEEE Trans. Components, Packag. Manuf. Technol.* **2014**, *4* (1), 46–56.

(64) Zhang, X. D.; Yang, X. H.; Zhou, Y. X.; Rao, W.; Gao, J. Y.; Ding, Y. J.; Shu, Q. Q.; Liu, J. Experimental Investigation of Galinstan Based Minichannel Cooling for High Heat Flux and Large Heat Power Thermal Management. *Energy Convers. Manag.* **2019**, *185*, 248–258.

(65) Zhu, J. Y.; Tang, S. Y.; Khoshmanesh, K.; Ghorbani, K. An Integrated Liquid Cooling System Based on Galinstan Liquid Metal Droplets. *ACS Appl. Mater. Interfaces* **2016**, *8* (3), 2173–2180.

(66) Chen, M.; Snyder, G. J. Analytical and Numerical Parameter Extraction for Compact Modeling of Thermoelectric Coolers. *Int. J. Heat Mass Transf.* **2013**, *60* (1), 689–699.

(67) Zhao, D.; Tan, G. A Review of Thermoelectric Cooling: Materials, Modeling and Applications. *Appl. Therm. Eng.* **2014**, *66* (1–2), 15–24.

(68) Pabst, W.; Hostaša, J. Thermal conductivity of ceramics-from monolithic to multiphase, from dense to porous, from micro to nano. *Advances in Materials Science Research. Nova Science*. **2011**, 1-112.

(69) Yu, B.; Xing, W.; Guo, W.; Qiu, S.; Wang, X.; Lo, S.; Hu, Y. Thermal Exfoliation of Hexagonal Boron Nitride for Effective Enhancements on Thermal Stability, Flame Retardancy and Smoke Suppression of Epoxy Resin Nanocomposites: Via Sol-Gel Process. *J. Mater. Chem. A* **2016**, *4* (19), 7330–7340.

(70) Kishore, R. A.; Nozariasbmarz, A.; Poudel, B.; Sanghadasa, M.; Priya, S. Ultra-High Performance Wearable Thermoelectric Coolers with Less Materials. *Nat. Commun.* **2019**, *10* (1), 1–13.

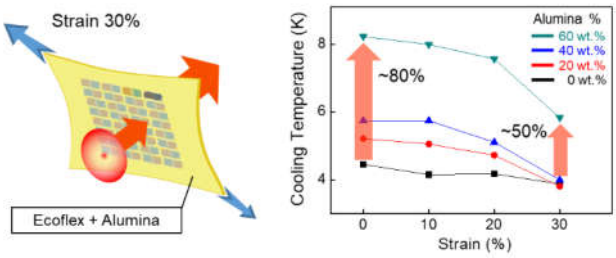

For Table of Contents Use Only